Dynamic Control of Axial Compressors*

Michael Larsen
Department of Electrical and Computer Engineering
University of California
Santa Barbara, CA 93106
larsenm@bode.ece.ucsb.edu

Brianno Coller
Control and Dynamical Systems, 116-81
California Inst. of Tech.
Pasadena, CA 91125
coller@cds.caltech.edu

Rodolphe Sepulchre
Institut Montefiore, B28
Université de Liège
B-4000 Liège Sart-Tilman
Belgium
sepulchre@montefiore.ulg.ac.be

Petar V. Kokotović
Department of Electrical and Computer Engineering
University of California
Santa Barbara, CA 93106
petar@ece.ucsb.edu

Abstract

Several control laws, for example [1, 2, 3], have been formulated to stabilize the low-order nonlinear state-space model of an axial compression system developed by Moore and Greitzer [4]. Using static nonlinear feedback, these control laws extend the stable operating range of the compressor system. This paper considers the merits of using dynamic feedback to implement the control law suggested by Sepulchre and Kokotović in [5]. Bifurcation and normal form analysis are used to show that the dynamic implementation of this control law is able to eliminate rotating stall by stabilizing a small axisymmetric limit cycle around the peak of the compressor characteristic. The analysis reveals the possibility that controlled dynamics can be used to create new and desirable phenomena.

1. Introduction

The performance of axial compressors is limited by two aerodynamic instabilities: rotating stall and surge. Rotating stall occurs when a mass of air becomes trapped in the blade passages of the compressor. This flow blockage, rotating around the compressor annulus, forces the compressor to operate at an undesirable reduced pressure. This instability is accompanied by hysteresis. Surge is characterized by large oscillations of the flow along the axial direction of the compressor

Moore and Greitzer [4] developed a PDE model for axial compression systems. Their model relates the pressure rise Ψ, annulus-averaged flow coefficient Φ, and disturbed flow coefficient of the compressor. Using a Galerkin approximation, a one-mode truncation yields a third order ODE:

$$\dot{\Phi} = -\Psi + \Psi_c(\Phi) - 3\Phi R \qquad (1..1a)$$

$$\dot{\Psi} = \frac{1}{\beta^2}(\Phi + 1 - \sqrt{\Psi}(\Gamma + u)) \qquad (1..1b)$$

$$\dot{R} = \sigma R(1 - \Phi^2 - R) \qquad (1..1c)$$

where $\Psi_c(\Phi)$ is the compressor characteristic. In this paper the cubic polynomial

$$\Psi_c(\Phi) = \Psi_0 + 1 + \frac{3}{2}\Phi - \frac{\Phi^3}{2} \qquad (1..2)$$

is used. R is the square magnitude of the first Fourier mode of the disturbed flow coefficient. The locus of equilibria of (1..1) for which $R \neq 0$, $\Psi = \Psi_c(\Phi) - 3\Phi(1-\Phi^2)$, is referred to as the stall characteristic. Steady axisymmetric (unstalled) flow corresponds to a stable equilibrium with $R = 0$ and steady non-axisymmetric (stalled) flow corresponds to a stable equilibrium with $R \neq 0$. The flow regime established in the compressor depends on the throttle opening Γ. Figures 1(a) and 1(c) are qualitative open loop bifurcation diagrams showing how the steady-state value of R, Φ, and Ψ vary with Γ. In Figure 1(c), we see that desirable steady axisymmetric flow loses stability at a bifurcation occurring at peak pressure rise resulting in a large pressure drop. Note also the hysteresis associated with the bifurcation as seen in Figure 1(c). A detailed bifurcation analysis of the the open loop behavior of (1..1) was done in [6].

This bifurcation cannot be eliminated with control. Because u enters into (1..1) through $\dot{\Psi}$, the locus of equilibria of (1..1), determined by varying Γ, is invariant with respect to u. Hence, from (1..1c) it is evident there will always be a bifurcation at the peak of the compressor characteristic $\Phi = 1, R = 0, \Phi = \Psi_c(1)$ irrespective of u. This bifurcation occurs at $\Gamma = \Gamma_{peak}$ where

$$\Gamma_{peak} = \frac{2}{\sqrt{\Psi_c(1)}} - u|_{\Phi=1,R=0,\Psi=\Psi_c(1)}. \qquad (1..3)$$

The control objective is thus to eliminate the hysteresis and reduce the large pressure drop caused by the open loop bifurcation. Liaw and Abed [7] showed that it is possible to use state feedback to change the nature of the bifurcation from subcritical to supercritical. The improvement achieved is seen in the the closed loop bifurcation diagrams of Figures 1(b) and 1(d). Other researchers proposed static nonlinear feedback control laws, for example [1, 2, 3], which not only soften the bifurcation but include terms to improve performance for nonlocal excursions of state variables and parameters. These designs achieve the control objective by stabilizing the non-axisymmetric (stalled) branch of equilibria that exists for $\Gamma < \Gamma_{peak}$. Since $R = 0$ is an invariant manifold regardless of the choice of u, equilibria in this manifold are uncontrollable. It is evident from (1..1c) that they posses an eigenvalue $(1 - \Phi_e^2)$, where Φ_e is the equilibrium value of Φ, which is

*This work was supported in part by AFOSR/PRET Grant 442530-25380

positive for $|\Phi_e| < 1$. Therefore it is not possible to stabilize the axisymmetric branch of equilibria for $\Gamma < \Gamma_{peak}$.

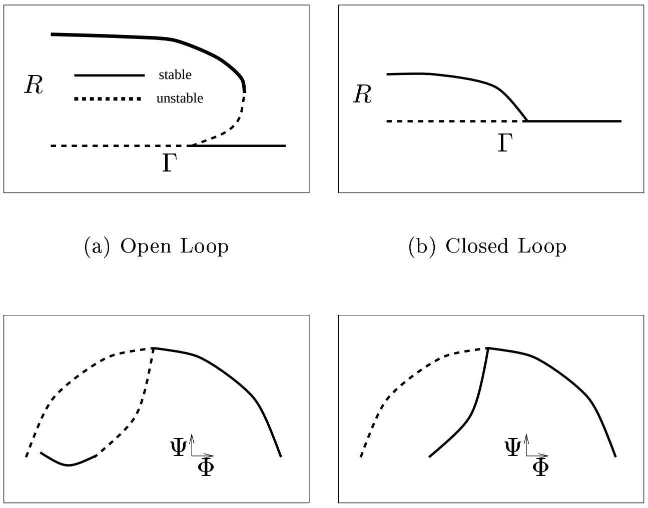

(a) Open Loop (b) Closed Loop

(c) Open Loop (d) Closed Loop

Figure 1: Bifurcation Control of Rotating Stall

2. Static S Control Law

By changing the nature of the bifurcation from subcritical to supercritical, the designs mentioned above reduce the steady state pressure drop caused by rotating stall. A linear analysis about an equilibrium on the stall characteristic shows that the zero dynamics of the output $\Psi - \Psi_e$ are unstable. The zero dynamics for this choice of output are

$$\begin{aligned} \dot{\Phi} &= -\Psi_e + \Psi_c(\Phi) - 3\Phi R && (2..4a) \\ \dot{R} &= \sigma R(1 - \Phi^2 - R) && (2..4b) \end{aligned}$$

Figure 2 is a plot of the eigenvalues of the linearized zero dynamics as Ψ_e is varied from $\Psi_e = \Psi_{peak} = 2.71875$ to $\Psi_e = 1.4$. Each value of Ψ_e in this range corresponds to a unique equilibrium on the stall characteristic. Since the linearized zero dynamics possess a positive eigenvalue, the zero dynamics are unstable. This non-minimum phase behavior constrains performance and motivates investigation of designs which minimize transient pressure loss.

To this end, Sepulchre and Kokotović [5] introduced control laws of the form

$$u = \frac{\Gamma_0 + k(\Psi - F(\Phi, R))}{\sqrt{\Psi}} - \bar{\Gamma}. \qquad (2..5)$$

The control forces a fast convergence of trajectories to the manifold $\Psi = F(\Phi, R)$. The set point of the controller is determined by Γ_0 and $\bar{\Gamma}$. A singular perturbation analysis of (1..1) with the control law defined by (2..5) reveals how F should be chosen to improve transient performance.

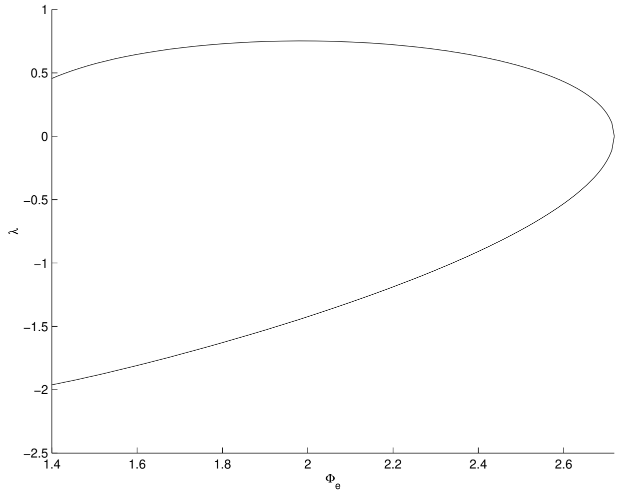

Figure 2: Eigenvalues of linearized zero dynamics of equilibria on the stall characteristic

For this purpose, we consider $\epsilon = 1/k$ to be small. This assumption allows us to use the tools of singular perturbation to study the geometric properties of (1..1). In many cases, these geometric properties remain valid for the usual values of the gain k. The closed loop system thus exhibits the singularly perturbed model

$$\begin{aligned} \dot{R} &= \sigma R(1 - \Phi^2 - R) && (2..6a) \\ \dot{\Phi} &= -\Psi + \Psi_c(\Phi) - 3\Phi R && (2..6b) \\ \epsilon\dot{\Psi} &= \frac{1}{\beta^2}(\epsilon(\Phi + 1 - \sqrt{\Psi}(\Gamma - \bar{\Gamma}) - \Gamma_0) \\ &\quad -(\Psi - F(\Phi, R))). && (2..6c) \end{aligned}$$

For ϵ sufficiently small, singular perturbation theory [8] guarantees the existence of an invariant manifold $\Psi = h(\Phi, R, \epsilon)$ to which Ψ will rapidly converge.

On the manifold, the dynamics of (2..6a) are slow, $0(1)$ or slower, as opposed to the dynamics off the manifold which are fast $0(\frac{1}{\epsilon})$. The location of the manifold is determined by the manifold condition

$$\dot{\Psi} = \epsilon(\frac{\partial h}{\partial \Phi}\dot{\Phi} + \frac{\partial h}{\partial R}\dot{R}). \qquad (2..7)$$

or

$$\begin{aligned} &\frac{1}{\beta^2}(\epsilon(\Phi + 1 - \sqrt{h(\Phi, R, \epsilon)}(\Gamma - \bar{\Gamma}) - \Gamma_0) - (h(\Phi, R, \epsilon) - F(\Phi, R))) \\ &= \epsilon(\frac{\partial h}{\partial \Phi}(-h(\Phi, R) + \Psi_c(\Phi) - 3\Phi R) + \frac{\partial h}{\partial R}(\sigma R(1 - \Phi^2 - R))) \\ &&& (2..8) \end{aligned}$$

For an $0(\epsilon^n)$-approximation of $h(\Phi, R, \epsilon)$, we substitute

$$h(\Phi, R, \epsilon) = h_0(\Phi, R) + \epsilon h_1(\Phi, R) + \cdots + \epsilon^{n-1}h_{n-1}(\Phi, R) + 0(\epsilon^n) \qquad (2..9)$$

into (2..7) and equate the terms of like powers of ϵ. For the problem at hand, this yields

$$h(\Phi, R, \epsilon) = F + \epsilon h_1 + 0(\epsilon^2) \qquad (2..10)$$

where

$$h_1 = \frac{\frac{\partial F}{\partial \Phi}(\Psi_c(\Phi) - 3\Phi R) + \sigma \frac{\partial F}{\partial R} R(1 - \Phi^2 - R) - \frac{1}{\beta^2}(\Phi + 1 - \sqrt{F}(\Gamma - \bar{\Gamma}) - \Gamma_0)}{\frac{\partial F}{\partial \Phi}}. \tag{2..11}$$

Hence F is an $0(\epsilon)$ approximation of the manifold to which Ψ converges and

$$\begin{aligned} \dot{R} &= \sigma R(1 - \Phi^2 - R) && (2..12) \\ \dot{\Phi} &= -F(\Phi, R) + \Psi_c(\Phi) - 3\Phi R && (2..13) \end{aligned}$$

is an $0(\epsilon)$ approximation of the dynamics on this manifold.

For the discussion to follow we define the functions $\Psi_s(\Phi)$ to be the Ψ along the locus of stabilizable equilibria of (1..1) and $\Psi_u(\Phi)$ to be the Ψ along the locus of equilibria that are not stabilizable, i.e.

$$\Psi_s(\Phi) = \begin{cases} \Psi_c(\Phi) & \text{when } \Phi \geq 1, \\ \Psi_c(\Phi) - 3\Phi(1 - \Phi^2) & \text{when } \Phi < 1 \end{cases}$$

and

$$\Psi_u(\Phi) = \Psi_c(\Phi) \text{ for } \Phi < 1.$$

The equilibria of (2..12) are determined by the intersection of F with $\Psi_s(\Phi)$ and $\Psi_u(\Phi)$. Let Φ_e be the value of Φ at the intersection of F with $\Psi_s(\Phi)$, assuming there is only one such intersection. Because of the ISS property of the stall dynamics, shown in [9], the equilibrium at Φ_e is asymptotically stable if

$$(\Phi - \Phi_e)(-F(\Phi, R_s(\Phi)) + \Psi_s(\Phi)) \geq 0$$

for all Φ where

$$R_s(\Phi) = \begin{cases} 0 & \text{when } \Phi \geq 1, \\ 1 - \Phi^2 & \text{when } \Phi < 1 \end{cases}$$

This constraint has a graphical interpretation shown in Figure 3. To achieve stability, the $F(\Phi, R_s(\Phi))$ must not lie in the hashed regions shown in Figure 3. In order to minimize the transient pressure drop when $\Phi < \Phi_e$, it is desirable that $F(\Phi, R_s(\Phi))$ be located close to $\Psi_s(\Phi)$.

It is also important to choose $F(\Phi, R_s(\Phi))$ so that the response the of the system to a throttle disturbance is attenuated. A typical disturbance can be modeled as a step variation $\delta\Gamma$ of Γ. The nominal operating point of the compressor system is designed to be a stable axisymmetric equilibrium to the right of the peak on the compressor characteristic. A negative throttle disturbance causes an undesirable shift of the operating point toward or even past the bifurcation point at the peak. Control laws that reduce this shift or that slow the drift of the system to the new operating condition are desirable.

These properties are achieved by the S control law described in [5]

$$u = \frac{\Gamma_0 + k(\Psi - \Psi_s(\Phi))}{\sqrt{\Psi}} - \bar{\Gamma}. \tag{2..14}$$

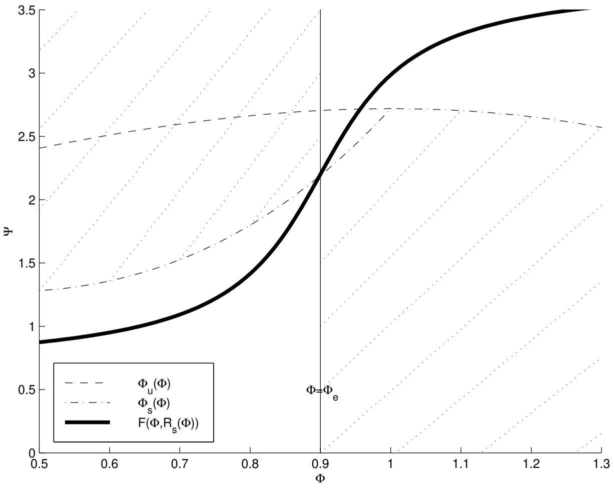

Figure 3: Stability quadrants for manifold placement

This control law forces the pressure to the slow manifold $\Psi_s(\Phi)$. The dynamics in the slow manifold are

$$\begin{aligned} \dot{R} &= \sigma R(1 - \Phi^2 - R) \\ \dot{\Phi} &= -(\Psi_s(\Phi) + \epsilon h_1) + \Psi_c(\Phi) - 3\Phi R \end{aligned}$$

or

$$\begin{aligned} \dot{R} &= \sigma R(1 - \Phi^2 - R) \\ \dot{\Phi} &= \begin{cases} -\epsilon h_1 - 3\Phi R & \text{for } \Phi > 1, \\ -\epsilon h_1 + 3\Phi(1 - \Phi^2 - R) & \text{for } \Phi \leq 1. \end{cases} \end{aligned} \tag{2..15}$$

From (2..15), we see that trajectories in the slow manifold converge with $0(1)$ to the sub-manifold made up of $R = 0$ for $\Phi > 1$ and $R = 1 - \Phi^2$ for $\Phi \leq 1$. In the slow sub-manifold $R = 1 - \Phi^2$, trajectories move with $0(\epsilon)$. For the throttle disturbance scenario with $\Gamma - \delta\Gamma < \Gamma_{peak}$ as described earlier, this results in a favorable transient response. The drift away from the nominal operating point to the stall equilibrium stabilized by the control law is $0(\epsilon)$. It is also evident from (2..15) that the saddle equilibrium is $0(\epsilon)$ from the peak. This further delays the drift from the nominal operating point to the stall equilibrium.

3. Dynamic S Control Law

Investigation of the performance of the S control law in the presence of actuator constraints (e.g. a time constant and a saturation limit) yielded unexpected results. With u defined by (2..14), we consider the control when it enters through a first order lag

$$\chi = \frac{1}{\tau s + 1} u. \tag{3..16}$$

This also can be viewed as a dynamic implementation of (2..14). With (3..16),

$$
\begin{aligned}
\dot{\Phi} &= -\Psi + \Psi_c(\Phi) - 3\Phi R && (3..17\text{a})\\
\dot{\Psi} &= \frac{1}{\beta^2}(\Phi + 1 - \sqrt{\Psi}(\Gamma + \chi)) && (3..17\text{b})\\
\dot{R} &= \sigma R(1 - \Phi^2 - R) && (3..17\text{c})\\
\tau\dot{\chi} &= u - \chi. && (3..17\text{d})
\end{aligned}
$$

Note that τ only affects the stability of the equilibria and not their location.

We present the results of a numerical simulation performed for (3..17) for a 5% throttle disturbance of Γ from Γ_{peak} for an initial condition at the peak, $\chi_0 = 0$, and a small initial perturbation of R. A saturation constraint was also imposed. Figure 4(a) shows the open loop performance of the system. The disturbance causes a large magnitude rotating stall to develop in 5 rotor rads. Figure 4(b) shows the closed performance for $\tau = 0$. The controller performs as expected. It reduces the steady state pressure loss caused by the disturbance without transient pressure loss. It also significantly delays the development of the stalled operating condition as seen in the difference in time scales of Figures 4(a) and 4(b). Figure 4(b) shows the closed performance for $\tau = 1$. The results are unexpected. The controller suppresses rotating stall and stabilizes a small limit cycle around the peak of the compressor characteristic. The limit cycle is shown in Figure 5. Even more surprising is the fact that this is achieved with less control effort in steady state than the control with $\tau = 0$ as seen in Figure 6.

This behavior does not occur for small τ. Treating τ as a small parameter, this system is in standard singularly perturbed form with the first three equations composing the slow subsystem with $\chi = u$. In [5] it was shown that the equilibrium of the slow subsystem is exponentially stable. It is clear that the equilibrium of the fast subsystem (3..17d) is also exponentially stable. Hence, by Thereom 9.3 of [10] the equilibrium of the whole system is locally exponentially stable for τ sufficiently small. This means that geometric properties of the controller for $\tau = 0$ are preserved, at least locally.

However, for larger τ the behavior of the system is radically different as evidenced by the numerical simulations. These results indicate that the control objective can be achieved with even further performance improvement, if we allow for the stabilization of more complex behavior, such as periodic orbits. This is illustrated by detailed study of the dynamic version of the S control law.

For $\Gamma < \Gamma_{peak}$ and $\tau = 0$, (3..17) has two equilibria in close proximity to each other. Both possess a pair of complex eigenvalues which migrate toward the $j\omega$ axis for $\tau > 0$. This reflects the surge dynamics,(3..17) when $R = 0$, present in the system. This manifold $R = 0$ is invariant and attractive for $\Phi < 1 - R^2$ where $\dot{R} < 0$ and

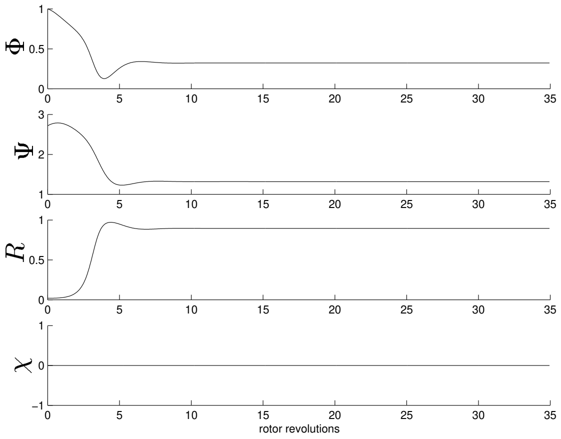

(a) Open Loop

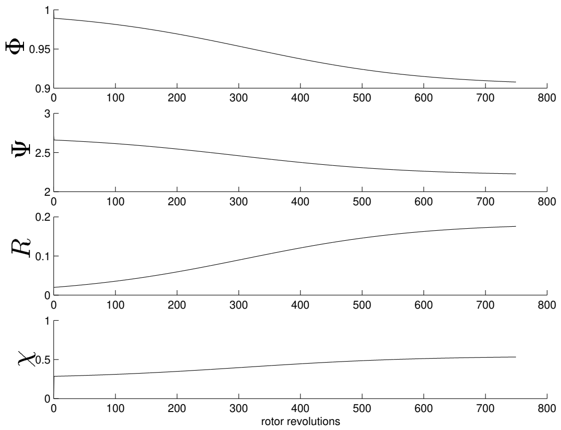

(b) Closed Loop $\tau = 0$

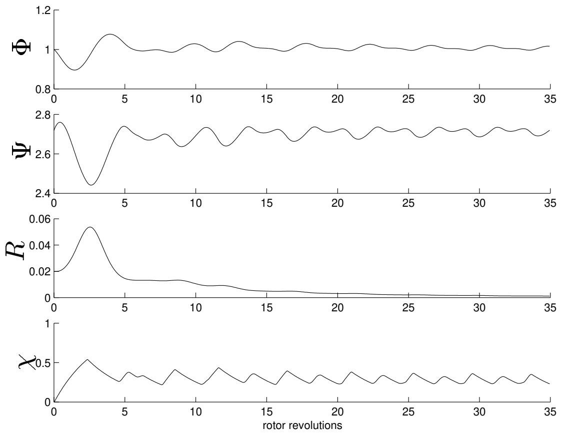

(c) Closed Loop $\tau = 1 > \tau_0$

Figure 4: Time Histories for a 5% Throttle Disturbance

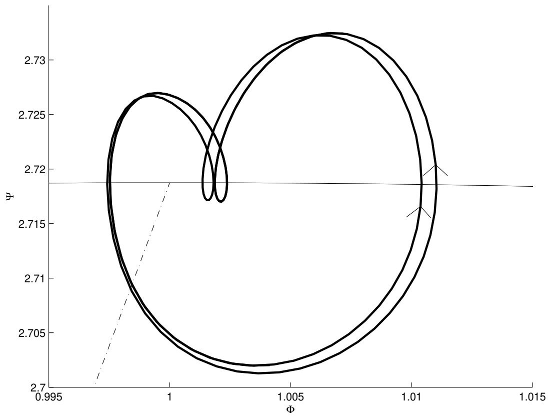

Figure 5: Zoom on limit cycle for $\tau = 1$

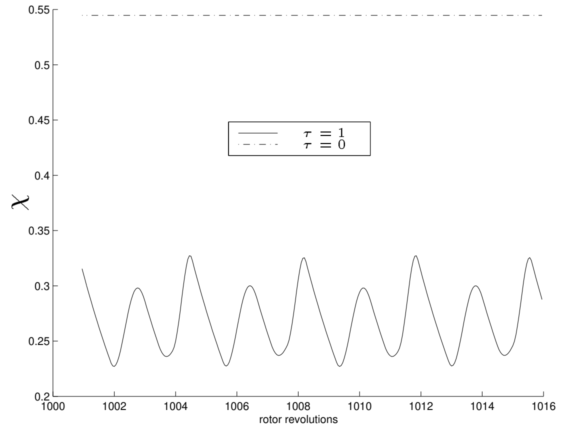

Figure 6: Comparison of Steady-State Control Effort

repelling for $\Phi > 1 - R^2$ where $\dot{R} < 0$. The attractive nature of the manifold is the underlying structure that changes the system's behavior. The proximity of the two equilibria and the fact that a pair of each's eigenvalues is weakly damped reveals a nonlinear interaction that cannot be analyzed by considering one alone.

3.1. Local Bifurcation Analysis

We proceed with a local bifurcation analysis with τ as the bifurcation parameter, for $\tau > 0$, about each of the equilibria. For a fixed $\Gamma < \Gamma_{peak}$, both equilibria undergo Hopf bifurcations. The Hopf bifurcation of the saddle occurring at τ_1 is subcritical and gives birth to a saddle limit cycle that lives in the manifold $R = 0$. The Hopf bifurcation of the rotating stall equilibrium occurring at τ_2 is supercritical and gives birth to a stable limit cycle. Figure 7 shows how τ_1 and τ_2 vary with Γ. As Γ is varied the location of the equilibria also change. The two branches of the bifurcation diagram merge at $\Gamma = \Gamma_{Peak}$. At this point, $\tau = \tau_{dnb}$, $\Gamma = \Gamma_{peak}$ a transcritical-Hopf bifurcation occurs. For $\Gamma > \Gamma_{peak}$, there is only one equilibrium that

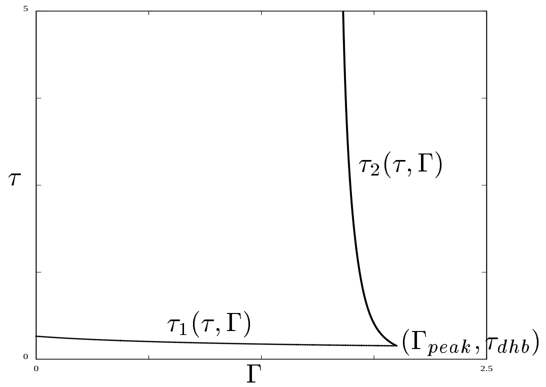

Figure 7: Hopf Bifurcations in τ,Γ parameter space

is physical. It is not destabilized by τ and so Figure 7 shows no Hopf bifurcation occuring for $\Gamma > \Gamma_{peak}$.

The fact that the equilibrium that exists for $\Gamma > \Gamma_{peak}$ does not undergo a Hopf bifurcation as τ is varied is a consequence of the sharp change of the control law that occurs at $\Phi = 1$. To capture the effect of this nonlinearity, we use a smooth approximation of $\Psi_s(\Phi)$ in u and perform a normal form analysis about $\tau = \tau_{dhb}$ and $\Gamma = \Gamma_{peak}$. The smooth approximation is required as the control law is not differentiable at $\Phi = 1$.

3.2. Normal Form Analysis

One of the authors has developed software to unfold Hopf-Hopf bifurcations. To make use of this machinery we first recast (3..17) in an equivalent form. Returning to the original PDE from which (3..17) was derived, we perform a Galerkin expansion of the magnitude and the phase of the first Fourier mode of the disturbed flow coefficient in complex form. This results in

$$\begin{aligned} \dot{\phi} &= f_\phi(\phi, \psi, z_1) && (3..18a) \\ \dot{\psi} &= f_\psi(\phi, \psi, z_1, \chi) && (3..18b) \\ \dot{z}_1 &= f_{z_1}(\phi, \psi, z_1) && (3..18c) \\ \tau\dot{\chi} &= f_\chi(\psi, u) && (3..18d) \end{aligned}$$

where $\phi = \Phi - \Phi_0$,$\psi = \Psi - \Psi_0$, and z_1 is a complex variable $z_1 = \sqrt{R}e^{j\theta}$ containing information about the magnitude and phase of the first mode of rotating stall. In this setting, the transcritical bifurcation occurring at $\Gamma = \Gamma_{peak}$ becomes a Hopf bifurcation. Instead of analyzing the transcritical-Hopf bifurcation, we analyze the equivalent Hopf-Hopf bifurcation of (3..18) and perturb off this doubly degenerate situation to discover the nearby behavior.

First, we compute the center manifold of (3..18) at the

Hopf-Hopf bifurcation up to cubic terms

$$\tilde{\chi} = h(\tilde{\phi}, \tilde{\psi}, \tilde{z}_1, \hat{\Gamma}, \hat{\tau}) + \mathcal{O}(4) \tag{3..19}$$

where $\hat{\Gamma} = \Gamma - \Gamma_{peak}$, $\hat{\tau} = \tau - \tau_{dhb}$, and $\tilde{\chi}$,$\tilde{\phi}$, $\tilde{\psi}$, and $\tilde{z}_1$ are defined by the linear transformation that is needed to decouple the linearization of (3..19) at the bifurcation point. Letting $z_0 = \tilde{\phi} + j\tilde{\psi}$, (3..18) on the center manifold is of the form

$$\begin{aligned} \dot{z}_0 &= \lambda_0 z_0 + f_0(z_0, z_1) \\ \dot{z}_1 &= \lambda_1 z_1 + f_1(z_0, z_1) \end{aligned} \tag{3..20}$$

where f_0 and f_1 are polynomials in z_0, z_0^*, z_1, z_1^*. The computation is done using MAPLE. To bring (3..20) into normal form we find functions h_0 and h_1, using MAPLE, such that the transformation

$$z_0 = a_0 + h_0(a_0, a_1) \tag{3..21}$$
$$z_1 = a_1 + h_1(a_0, a_1) \tag{3..22}$$

yields

$$\begin{aligned} \dot{a}_0 &= a_0(\lambda_0 + b_{00} a_0 a_0^* + b_{01} a_1 a_1^*) + \mathcal{O}(5) \\ \dot{a}_1 &= a_1(\lambda_1 + b_{10} a_0 a_0^* + b_{11} a_1 a_1^*) + \mathcal{O}(5). \end{aligned} \tag{3..23}$$

The complex variables a_0 and a_1 are essentially the surge (Φ,Ψ) and the stall (z_1) variables respectively. Considering only the magnitudes of a_0 and a_1 and rescaling them appropriately, we arrive at the Hopf-Hopf normal form found in [11]

$$\begin{aligned} \dot{r}_0 &= r_0(\mu_0 + r_1^2 + b r_2^2) \\ \dot{r}_1 &= r_1(\mu_1 + c r_1^2 + d r_2^2). \end{aligned} \tag{3..24}$$

The equilibrium at the origin corresponds to the axisymmetric equilibrium of (3..18). An equilibrium of (3..24) with $r_0 = 0, r_1 \neq 0$ corresponds to a non-axisymmetric limit cycle of (3..18) or relative equilibria of (3..17), i.e. stall. An equilibrium of (3..24) with $r_1 = 0, r_0 \neq 0$ corresponds to an axisymmetric limit cycle of (3..18), i.e. surge-like behavior. The unfolding of (3..24) gives the parameters μ_0,μ_1 and b, c, d in terms of $\hat{\Gamma}$ and $\hat{\tau}$ and is done using MAPLE.

The resulting unfolding diagram shown in Figure 8 along with corresponding phase portraits in Figure 9 render a qualitative description of the dynamics near the Hopf-Hopf bifurcation. Portraits I-III, confirm the local bifurcation analysis performed around the each of the equilibrium of (3..17). The equilibrium bifurcate and give birth to limit cycles (or tori in context of (3..18)). Moving from portraits III to IV, the axisymmetric limit cycle acquires stability as it bifurcates with a torus. Outside of regions I-VI, the dynamics of (3..17) are not captured by the center manifold. Region VI exists as a result of the approximation of $\Psi_s(\Phi)$. As noted previously, the axisymmetric equilibrium does not undergo a Hopf bifurcation as τ increases for $\Gamma > \Gamma_{peak}$.

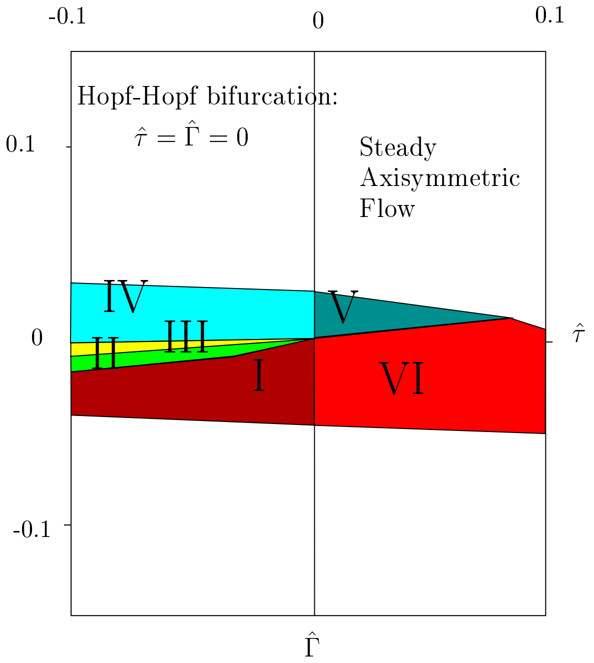

Figure 8: Unfolding Diagram

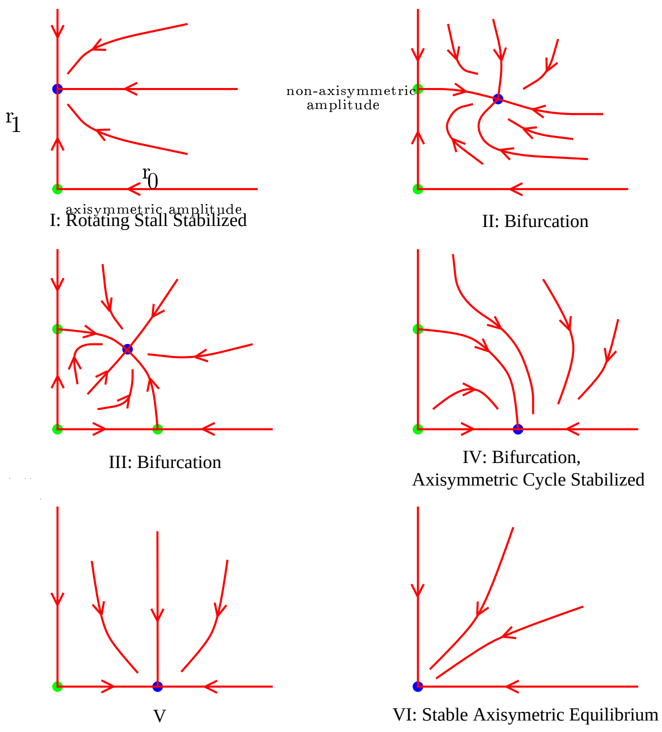

Figure 9: Phase Portraits

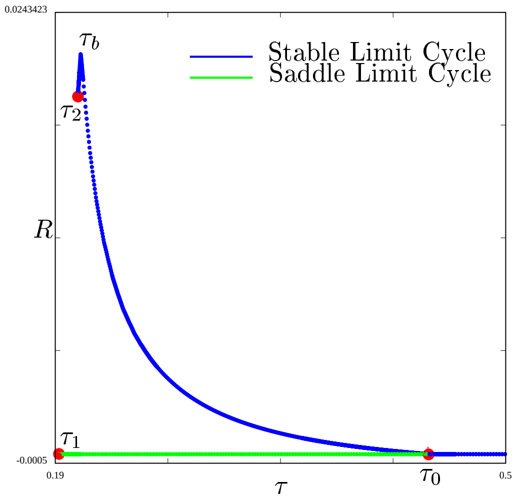

Figure 10: Branch Tracking of Periodic Orbits

To demonstrate that the results of the normal form analysis hold for the non-smooth control law, we use DsTool along with CANDYS/QA to numerically track some of the the branches of periodic orbits emmanating from Hopf bifurcations found in the local bifurcation analysis. This is done to analyze how the periodic orbit changes with τ is varied for a fixed Γ. In the bifurcation diagram of Figure 10, for a fixed τ, each point represents a periodic orbit. The vertical axis is the maximum value of R obtained by the periodic orbit as τ is varied. At $\tau = \tau_b$, the effect of the non-smooth kink in the control is seen in the sharp bend in the branch of stable periodic orbits emanating from the equilibrium with $R \neq 0$. Just as predicted by the normal form analysis, the periodic orbits coalesce, resulting in a stable axisymmetric limit cycle for $\tau > \tau_0$. The size of this periodic orbit is small. Figure 11 shows the phase portraits of some of the periodic orbits as τ is varied.

The reason for this behavior is the interaction of the manifold $R = 0$ and the strong nonlinearity in the control law at $\Phi = 1$. For $\Gamma < \Gamma_{peak}$, there are two equilibria with $\Phi < 1$. Under the action of the control law, each equilibrium has a pair of poorly damped complex eigenvalues for $\tau = 0$. Increasing τ destabilizes the equilibria resulting in periodic behavior around the equilibria. As τ is further increased, the periodic orbits would grow large without the

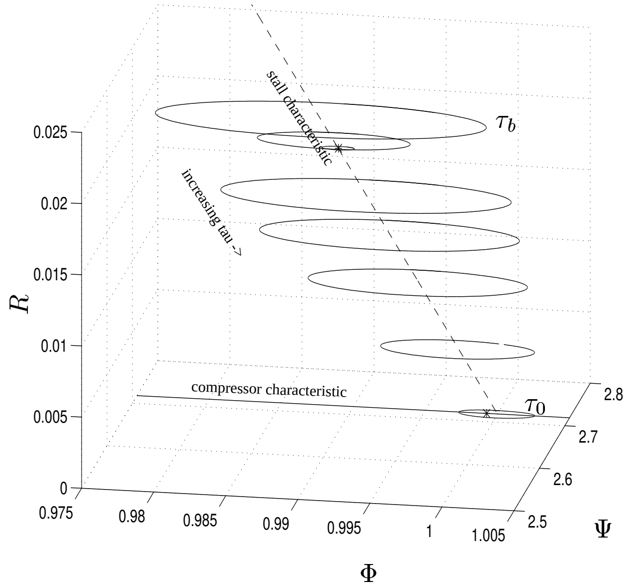

(a)

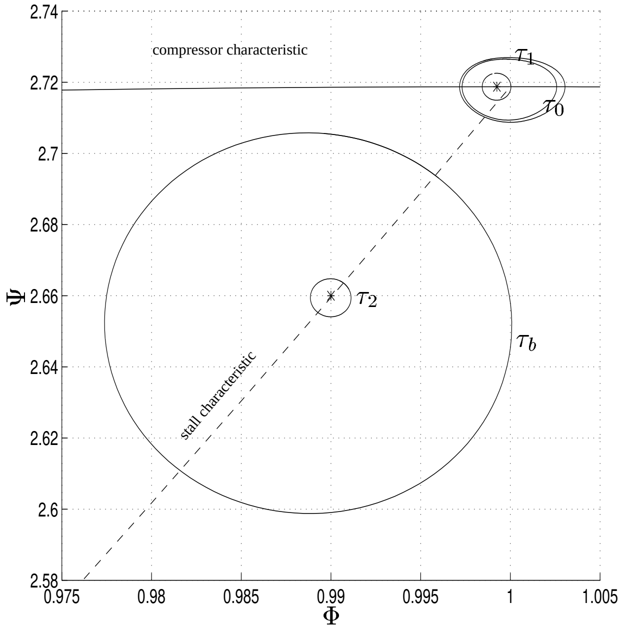

(b)

Figure 11: Limit Cycles

non-smooth deformation of the control at $\Phi = 1$. With the deformation, the control damps the periodic motion in such a way that a small periodic orbit is captured by the manifold $R = 0$ under the manifold's attractive influence which exists for $\Phi > 1 - R^2$.

4. Conclusion

Previous designs avoid hysteresis and reduce pressure loss through stabilization of a relative equilibrium near the peak of the compressor characteristic corresponding to a non-axisymmetric limit cycle. The dynamic version of the S control law further reduces the pressure loss through stabilization of a small axisymmetric limit cycle around the peak of the compressor characteristic. The location of this limit cycle is desirable as it corresponds to a steady-state solution maintaining maximal pressure rise without rotating stall. The resulting closed loop bifurcation diagram is shown in Figure 12. For nonlinear systems, this indicates the possibility that performance may be improved by stabilizing more complex behavior such as periodic orbits instead of stabilizing an equilibrium.

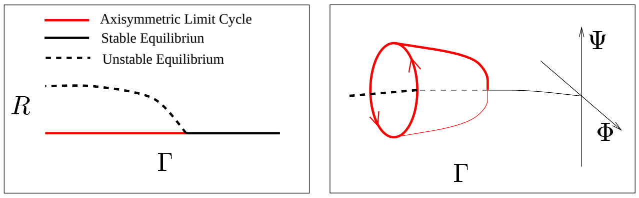

(a) Closed Loop $\tau > \tau_0$ (b)

Figure 12: Bifurcation control with the dynamic S control law

References

[1] K.M. Evecker, D.L. Gysling, C.N. Nett, and O.P. Sharma. Integrated control of rotating stall and surge in aeroengines. In *SPIE Conference on Sensing, Actuation and Control in Aeropropulsion*, 1995.

[2] M. Krstic, J.M. Protz, J.D. Paduano, and P.V. Kokotović. Backstepping designs for jet engine stall and surge control. In *Proc. of the 34th IEEE Conf. on Decision and Control*, pages 3049–3055, 1995.

[3] H.O. Wang, R.A. Adomatis, and E.H. Abed. Nonlinear analysis and control of rotating stall in axial flow compressors. In *Proceedings of the American Control Conference*, pages 2317–2321, 1994.

[4] F. K. Moore and E.M. Greitzer. A theory of post-stall transients in axial compressors: Part I - development of the equations. *AMSE Journal of Engineering for Gas Turbines and Power*, 108:68–76, 1986.

[5] Rodolphe Sepulchre and Petar Kokotović. Asymptotic methods for nonlinear control: a jet engine case study. UCSB Technical Report CCEC-960220.

[6] F. E. McCaughan. Bifurcation analysis of axial flow compressor stability. *SIAM Journal of Applied Math.*, 50(1232-1253), October 1990.

[7] D. C. Liaw and E. H. Abed. Active control of compressor stall inception: a bifurcation-theoretic approach. *Automatica*, 32:109–115, 1996. also in *Proceeding of the IFAC Nonlnear Control Systems Design Symposium*, Bordeaux, France, June 1992.

[8] P. Kokotović, H. Khalil, and J. O'Reilly. *Singular perturbation methods in control: analysis and design.* Academic Press, 1986.

[9] Krstić and et al. Useful nonlinearities and global bifurcation control of jet engine surge and stall. Submitted to *IEEE Transactions on Automatic Control.*

[10] Hassan K. Khalil. *Nonlinear Systems.* Prentice Hall, 1996.

[11] John Guckenheimer and Philip Holmes. *Nonlinear Oscillations, Dynamical Systems, and Bifurcation of Vector Fields.* Springer-Verlag, 1983.